

Adomian Decomposition Based Numerical Scheme for Flow Simulations

Imanol Garcia-Beristain^a, Lakhdar Remaki^{a,b}

^a*BCAM - Basque Center for Applied Mathematics, Alameda Mazarredo 14, 48009, Bilbao, Spain*

^b*Department of Mathematics and Computer Science, Alfaisal University, KSA*

Abstract

Time efficiency is one of the more critical concerns in computational fluid dynamics simulations of industrial applications. Extensive research has been conducted to improve the underlying numerical schemes to achieve time process reduction. Within this context, this paper presents a new time discretization method based on the Adomian decomposition technique for Euler equations. The obtained scheme is time-order adaptive; the order is automatically adjusted at each time step and over the space domain, leading to significant processing time reduction. The scheme is formulated in an appropriate recursive formula, and its efficiency is demonstrated through numerical tests by comparison to exact solutions and the popular Runge-Kutta-DG method.

Keywords: Adomian decomposition, Euler equations, Linearized Euler Equations, Aeroacoustics, Discontinuous Galerkin (DG)

I. Introduction

Computational fluid dynamics (CFD) is the numerical simulation of fluid flow, heat and mass transfer, turbulence, and other physical properties of fluids. This is achieved by solving Euler equations numerically for inviscid flows and Navier-Stokes equations for viscous flows. Details of the involved equations from modelling to numerical discretization can be found in [1, 2, 3].

Email addresses: igarcia@bcamath.org (Imanol Garcia-Beristain), lremaki@bcamath.org (Lakhdar Remaki)

CFD is extensively used in a wide range of industrial sectors including aeronautics and automotive [4, 5, 6, 7], ventilation and gas turbine design [8, 9, 10, 11, 12, 13], chemical manufacturing [14], oil industry [15], power generation and marine energy [16], food processing [17, 18], water treatment [19], and others. An interesting overview of the application of CFD to industrial applications is provided in [20, 21]. To illustrate this fact, one can mention, for instance, that wind tunnel testing in automotive and aeronautics sectors is strongly combined with CFD simulations for better and cost-effective results and bringing products to market faster. The exclusive use of CFD appears as a serious option in the near future. Bloodhound supersonic car fully designed with CFD is a good example of this trend[7, 22].

Aeroacoustics simulations, referred to by computational aeroacoustic (CAA), are among the most important CFD applications. The main objective of such simulations is noise reduction based on an accurate noise prediction. Reducing noise is of great importance for industry and human life quality. In transportation, a sensitive population's mobility growth is expected thanks to fast transportation facilities' development. In the US, the Joint Planning and Development Office (JPDO) is creating a new NextGen system plan for an expected air traffic increase by a factor of 3 towards 2025. Therefore reducing harmful sound effects becomes critical. A study of the impact of industrial noise on human life can be found in [23, 3].

One of the most challenging aspects when dealing with a numerical discretization of Euler and Navier-Stokes equations is the time efficiency. Indeed in industrial applications, complex geometries are used for simulations resulting in big meshes size that significantly increases the processing time. The case of aeroacoustics applications is even worse; a very fine mesh, around 6 points per wavelength, is required, aggravated by the need for extended time propagation resulting in the use of large domains, adding to that the significant scale differences inherent to the nature of the phenomenon [24].

CAA simulations can be classified into two categories: *direct noise computation* (DNC) and *hybrid methods* [25]. DNC method computes simultaneously acoustic and aerodynamic fields using compressible Navier-Stokes or Euler equations. The DNC requires low dispersive

and low dissipative numerical methods, making the approach prohibitively expensive in terms of computational cost; consequently, its use limited for real-life applications [25]. On the contrary, the hybrid method computes the aerodynamic and the acoustic fields in two separate steps, following Lighthill’s *acoustic analogy* [26, 27]. The approach requires first solving the aerodynamic field, used to evaluate an acoustical source that is then propagated. Linearised Euler equations (LEE) or nonlinear Euler equations [28], where the fluid is decomposed into a mean flow part and perturbation part, are the standard ways used to propagate the acoustic field. Most industrial CAA applications favor the hybrid method and often use LEE decomposition being faster and more robust than its nonlinear alternative [28, 29, 30, 31]. Hybrid methods are significantly cost-effective compared to DNC, and are mostly adopted in aeronautics [28, 32]. Nevertheless, they still requiring high-order low-dispersion schemes, and hence long simulation time [31]. In a conclusion, LEE is extensively used for aeroacoustic waves simulations due to the many advantages this approach offers [29, 30, 31]. Indeed, LEE in addition of being significantly faster than nonlinear Euler Equations, advection velocity, and amplitude, are easier to preserve by performing a linearization around the mean flow. In contrast, nonlinear Euler equations might completely damp waves by numerical diffusion. From another side, the information about the mean flow is preserved compared to a simple wave equation. Consequently, LEE offers a good compromise between simple wave propagation equations and nonlinear equations. Despite the linear nature of the LEE, due to the big required domains and very fine mesh, existing numerical methods need to be significantly improved especially for high-order methods.

Reducing computational time for high-order methods is a very active research field [33]. A significant effort is put into the implementation aspect using parallel architectures to attenuate the prohibitive time processing [34, 35]. In parallel, considerable work is devoted to improving numerical schemes based on adaptivity techniques to avoid unnecessary computations.

Two main adaptive strategies are developed in literature; mesh adaptivity, referred to by *h*-adaptivity, where the mesh quality is improved by performing local operations on mesh cells

and based on a selected metric. The operations include refinement, swapping, and coarsening [36, 37, 38, 39, 40]. The other strategy, referred to by p -adaptivity, consists of adapting the method order. Although order adaptivity is widely used in space [41, 42], it has not been reported in time adaptivity, except adjustment of time-step size [43, 44].

Within this context, this paper tries to open doors to build cost-effective time-adaptive (p -adaptivity) numerical schemes through the semi-analytical Adomian decomposition technique for Euler Equations. Adomian decomposition method first proposed by Adomian [45, 46, 47], is used by many authors to solve a big range of problems covering linear and nonlinear PDEs either deterministic or stochastic. This demonstrates that the approach is a promising trend in the field of approximation of PDEs solutions. See, for instance, the important work of Wazwaz [48, 49, 50, 51, 52, 53, 54, 53], and other relevant articles [55, 56, 57]. The reader is particularly referred to the nice review paper by Duan et al [49].

While almost all the work on Adomian decomposition in the literature focuses on finding semi-analytical solutions for PDEs (very limited work on CFD), we investigate the potential of using this technique to build efficient numerical schemes.

Very few works can be found on semi-analytical CFD solutions; we can cite solving Burgers' equation [58, 59, 60], and fractional derivative type problems such as the fractional Navier-Stokes equations [54, 53]. This approach, however, is too prohibitive to be used for complex real-life problems. Indeed, the approach calculates successive Adomian series terms analytically, which become exponentially complex even for simple problems. Only the very few first terms can be actually calculated, resulting in a significant truncation error.

The use of Adomian decomposition to derive numerical schemes is even rarer; one can cite the work about the fractional Navier-Stokes equations [61]. Here the method is applied to discrete Navier-Stokes. In other words, a Cartesian mesh is used for space discretization, which is a severe limitation for real applications that uses complex CADs (computer-aided design) where unstructured meshes are required. Moreover the *Riemann-Liouville* integrals are used for time increment, which is numerically prohibitive. This makes the method not competitive compared to standard numerical methods.

The novelty of the present work can be summarized as follows; first, the proposed numerical method uses the same data structure used for standard numerical methods like finite element, finite volume, discontinuous Galerkin(DG) methods, and so on. Consequently, no extra complexity is required, and the method can be implemented in any existing CFD platform (commercial, open-source, or academic). Second, the method is time-exact, with no need for any integration formula. Finally, the method is time-adaptive which can sensibly improve the cost-effectiveness of existing space-discretization methods.

To derive the proposed method, the semi-analytical Adomian decomposition technique is applied to the Euler equations. By considering the decomposition at each time step, a time discretization scheme is obtained. A recursive formula is established and proved providing a simple and practical formulation of the scheme. We refer to the obtained method by ABS standing for Adomian Based Scheme. The most important property of the scheme is its local time-order adaptivity, in the sense that the order is automatically adjusted at each time step and over the whole space domain, conferring to the method its time-effectiveness.

Space discretization can be achieved by any standard method. In this work classical discontinuous Galerkin (DG) approach is selected, and ABS-DG is used to refer to the full discretization. Numerical tests are performed using ABS-DG and Runge-Kutta - DG (RK-DG), and then results are compared to demonstrate the performance of the proposed method. A comparison to exact solutions is also presented.

In section 2, a short overview of the Adomian decomposition method and the nonlinear Euler and linearized Euler equations (LEE) are given. In section 3, details of the proposed ABS and ABS-DG schemes are provided as well as a stability analysis. In section 4, the connection of ABS-DG to the Runge-Kutta (RK) in the linear case is established. Tests are performed and reported in section 5.

II. Adomian Decomposition Overview

II.I. The Adomian Decomposition Method

In the following, a short description of the Adomian decomposition method is provided, for more details see [46, 45, 49].

Given a differential equation, the method consists in decomposing the equation as follows,

$$L(u) + R(u) + N(u) = 0, \quad (1)$$

where u is the unknown, L and R are the linear parts of the differential operator, with L being the easily invertible part. N is the nonlinear part.

Note that it is not necessary to distinguish the non-invertible linear part from the non-linear one. The sum $N + R$ can be represented by a single operator N , reducing the decomposition to

$$L(u) + N(u) = 0, \quad (2)$$

then the solution u and the operator N are expanded as,

$$u = \sum_{n=0}^{\infty} u_n, \quad (3)$$

and

$$N = \sum_{n=0}^{\infty} N_n. \quad (4)$$

The Adomian polynomial coefficients N_n are given by

$$N_n = \frac{1}{n!} \frac{\partial^n}{\partial \lambda^n} \left[N \left(\sum_{k=0}^n \lambda^k u_k \right) \right]_{\lambda=0}, \quad (5)$$

and the terms u_n of the series are computed as follows

$$u_{n+1} = L^{-1}(N_n). \quad (6)$$

II.II. The non-conservative Euler equations

The two-dimensional compressible inviscid flow equations (Euler equations) formulated relative to a Cartesian (x, y) coordinates system, in primitive variables, are given by

$$\begin{cases} \partial_t(\rho) + \partial_x(\rho u) + \partial_y(\rho v) = 0 \\ \partial_t(u) + u\partial_x(u) + v\partial_y(u) + \frac{1}{\rho}\partial_x p = 0 \\ \partial_x(v) + u\partial_x(v) + v\partial_y(v) + \frac{1}{\rho}\partial_y p = 0 \\ \partial_x(p) + u\partial_x(p) + v\partial_y(p) + \gamma p(\partial_x(u) + \partial_y(v)) = 0, \end{cases} \quad (7)$$

where ρ and p denote the averaged density and pressure of the fluid respectively and u_α is the averaged velocity of the fluid in direction x_α . Solutions to the set of equations are defined on a fixed spatial computational domain Ω .

Euler equations can also be written in a vector form,

$$\frac{\partial Q}{\partial t} + \mathcal{A} \frac{\partial Q}{\partial x} + \mathcal{B} \frac{\partial Q}{\partial y} = 0, \quad (8)$$

where, $Q = (\rho, u_1, u_2, p)^t$ and

$$\mathcal{A}(x, y, t) = \begin{pmatrix} u & \rho & 0 & 0 \\ 0 & u & 0 & 1/\rho \\ 0 & 0 & u & 0 \\ 0 & \rho c^2 & 0 & u \end{pmatrix} \quad \mathcal{B}(x, y, t) = \begin{pmatrix} v & 0 & \rho & 0 \\ 0 & v & 0 & 0 \\ 0 & 0 & v & 1/\rho \\ 0 & 0 & \rho c^2 & v \end{pmatrix}, \quad (9)$$

where $c^2 = \gamma \frac{p}{\rho}$ is the sound speed.

II.III. The Linearized Euler Equations (LEE)

LEE system is obtained by a linearization around a mean flow. This is achieved by decomposing the solution into mean and perturbation parts $Q = Q_0 + Q'$ then substituting

in equation (8) and assuming that

$$\frac{\partial Q_0}{\partial t} + \mathcal{A}_0 \frac{\partial Q_0}{\partial x} + \mathcal{B}_0 \frac{\partial Q_0}{\partial y} = 0, \quad (10)$$

with \mathcal{A}_0 and \mathcal{B}_0 the matrices \mathcal{A} and \mathcal{B} evaluated at Q_0 .

We obtain [62, 63, 64],

$$\frac{\partial Q'}{\partial t} + \mathcal{A}_0 \frac{\partial Q'}{\partial x} + \mathcal{B}_0 \frac{\partial Q'}{\partial y} + \mathcal{A}' \frac{\partial Q_0}{\partial x} + \mathcal{B}' \frac{\partial Q_0}{\partial y} = 0, \quad (11)$$

where $Q' = (\rho', u', v', p')^t$ and \mathcal{A}' and \mathcal{B}' are the matrices \mathcal{A} and \mathcal{B} evaluated at Q' .

For a smooth background (mean flow) which implies that mean flow spatial derivatives are moderate, in the sense

$$\mathcal{A}' \frac{\partial Q_0}{\partial x} \ll \mathcal{A}_0 \frac{\partial Q'}{\partial x}, \quad \text{and} \quad \mathcal{B}' \frac{\partial Q_0}{\partial y} \ll \mathcal{B}_0 \frac{\partial Q'}{\partial y}, \quad (12)$$

equation (11) is simplified to

$$\frac{\partial Q'}{\partial t} + \mathcal{A}_0 \frac{\partial Q'}{\partial x} + \mathcal{B}_0 \frac{\partial Q'}{\partial y} = 0. \quad (13)$$

In this paper, matrices \mathcal{A}_0 and \mathcal{B}_0 are considered to be constant (a common simplification in aeroacoustics) without loss of generality. For convenience, the prime symbol is dropped from Q' .

III. Adomian Based Schemes (ABS)

In this section, a cost-effective numerical scheme to solve nonlinear Euler Equations is derived. The time discretization is obtained using the Adomian decomposition technique, while the DG method (any other discretization method can be used) is applied for the space discretization. We refer to the semi-discretized scheme by ABS standing for Adomian Based

Scheme, and by ABS-DG to the fully-discretized scheme. The DG space discretization is implemented following the approach proposed by Shu [65]. For other classical DG discretizations, the reader is referred to Cockburns paper [66].

III.I. ABS Scheme Derivation

To apply the Adomian decomposition technique described in section II.I to Euler equations (7), we propose to set

$$L = \frac{\partial}{\partial t} \quad \text{and then} \quad L^{-1} = \int_0^t ds.$$

The nonlinear operator N is given by the remaining terms,

$$N(Q) = \mathcal{A}(Q) \frac{\partial Q}{\partial x} + \mathcal{B}(Q) \frac{\partial Q}{\partial y} \quad (14)$$

with Q being the primitive variables

$$Q = \begin{pmatrix} \rho \\ u \\ v \\ p \end{pmatrix}. \quad (15)$$

First Q is expanded as in (3)

$$Q = \sum_{n=0}^{\infty} Q_n, \quad (16)$$

the Adomian coefficients (4) are then give by

$$N_n = \frac{1}{n!} \frac{\partial^n}{\partial \lambda^n} \left[\mathcal{A} \left(\sum_{k=0}^n \lambda^k Q_k \right) \frac{\partial}{\partial x} \left(\sum_{k=0}^n \lambda^k Q_k \right) + \mathcal{B} \left(\sum_{k=0}^n \lambda^k Q_k \right) \frac{\partial}{\partial y} \left(\sum_{k=0}^n \lambda^k Q_k \right) \right]_{\lambda=0}, \quad (17)$$

which yields

$$N_n = \frac{1}{n!} \frac{\partial^n}{\partial \lambda^n} \left[\begin{array}{l} \partial_x \left(\left(\sum_{k=0}^n \lambda^k \rho_k \right) \left(\sum_{k=0}^n \lambda^k u_k \right) \right) \\ \quad + \partial_y \left(\left(\sum_{k=0}^n \lambda^k \rho_k \right) \left(\sum_{k=0}^n \lambda^k v_k \right) \right) = 0 \\ \\ \left(\sum_{k=0}^n \lambda^k u_k \right) \partial_x \left(\sum_{k=0}^n \lambda^k u_k \right) + \left(\sum_{k=0}^n \lambda^k v_k \right) \partial_y \left(\sum_{k=0}^n \lambda^k u_k \right) + \\ \quad \left(\frac{1}{\sum_{k=0}^n \lambda^k \rho_k} \right) \partial_x \left(\sum_{k=0}^n \lambda^k p_k \right) = 0 \\ \\ \left(\sum_{k=0}^n \lambda^k u_k \right) \partial_x \left(\sum_{k=0}^n \lambda^k v_k \right) + \left(\sum_{k=0}^n \lambda^k v_k \right) \partial_y \left(\sum_{k=0}^n \lambda^k v_k \right) + \\ \quad \left(\frac{1}{\sum_{k=0}^n \lambda^k \rho_k} \right) \partial_y \left(\sum_{k=0}^n \lambda^k p_k \right) = 0 \\ \\ \left(\sum_{k=0}^n \lambda^k u_k \right) \partial_x \left(\sum_{k=0}^n \lambda^k p_k \right) + \left(\sum_{k=0}^n \lambda^k v_k \right) \partial_y \left(\sum_{k=0}^n \lambda^k p_k \right) + \\ \quad \gamma \left(\sum_{k=0}^n \lambda^k p_k \right) \left(\partial_x \left(\sum_{k=0}^n \lambda^k p_k \right) + \partial_y \left(\sum_{k=0}^n \lambda^k v_k \right) \right) = 0 \end{array} \right]_{\lambda=0}.$$

The series terms Q_{n+1} are computed recursively by (6),

$$Q_{n+1}(x, y, t) = \int_0^t N_n(x, y, t) ds, \quad (18)$$

with N_n a four components vector

$$N_n = \begin{pmatrix} A_n \\ B_n \\ C_n \\ D_n \end{pmatrix}. \quad (19)$$

Let's develop the first component A_n , corresponding to the continuity equation.

From (17)

$$A_n(x, y, t) = \frac{1}{n!} \frac{\partial^n}{\partial \lambda^n} \left[\frac{\partial}{\partial x} \left(\left(\sum_{k=0}^n \lambda^k \rho_k \right) \left(\sum_{k=0}^n \lambda^k u_k \right) \right) + \frac{\partial}{\partial y} \left(\left(\sum_{k=0}^n \lambda^k \rho_k \right) \left(\sum_{k=0}^n \lambda^k v_k \right) \right) \right]_{\lambda=0}.$$

In the first summation part of A_n , permute the order of the derivatives (assuming the required

regularity to do so)

$$\frac{1}{n!} \frac{\partial^n}{\partial \lambda^n} \left[\frac{\partial}{\partial x} (\cdot) \right]_{\lambda=0} = \frac{1}{n!} \frac{\partial}{\partial x} \left[\frac{\partial^n}{\partial \lambda^n} (\cdot) \right]_{\lambda=0}.$$

Using the *Leibniz* formula, we get

$$\frac{\partial^n}{\partial \lambda^n} \left(\sum_{k=0}^n \lambda^k \rho_k \sum_{k=0}^n \lambda^k u_k \right) = \sum_{j=0}^n \binom{j}{k} \frac{\partial^{n-j}}{\partial \lambda^{n-j}} \left(\sum_{k=0}^n \lambda^k \rho_k \right) \frac{\partial^j}{\partial \lambda^j} \left(\sum_{k=0}^n \lambda^k u_k \right).$$

Note that

$$\frac{\partial^{n-j}}{\partial \lambda^{n-j}} \left(\sum_{k=0}^n \lambda^k \rho_k \right) \Big|_{\lambda=0} = (n-j)! \rho_{n-j}, \quad \text{and} \quad \frac{\partial^j}{\partial \lambda^j} \left(\sum_{k=0}^n \lambda^k u_k \right) \Big|_{\lambda=0} = (j)! u_j,$$

we then obtain

$$\frac{1}{n!} \frac{\partial}{\partial x} \left[\frac{\partial^n}{\partial \lambda^n} \left(\left(\sum_{k=0}^n \lambda^k \rho_k \right) \left(\sum_{k=0}^n \lambda^k u_k \right) \right) \right]_{\lambda=0} = \sum_{j=0}^n \frac{\partial}{\partial x} (\rho_{n-j} u_j). \quad (20)$$

Similarly, the second summation part is simplified as,

$$\frac{1}{n!} \frac{\partial}{\partial y} \left[\frac{\partial^n}{\partial \lambda^n} \left(\left(\sum_{k=0}^n \lambda^k \rho_k \right) \left(\sum_{k=0}^n \lambda^k v_k \right) \right) \right]_{\lambda=0} = \sum_{j=0}^n \frac{\partial}{\partial y} (\rho_{n-j} v_j). \quad (21)$$

Substituting (20), (21) into A_n , we get the formula

$$A_n = - \sum_{j=0}^n (\partial_x (\rho_{n-j} u_j) + \partial_y (\rho_{n-j} v_j)). \quad (22)$$

A similar formula for D_n is obtained by repeating the same steps.

For B_n and C_n , first expand $\frac{1}{\sum_{k=0}^n \lambda^k \rho_k}$ as power series (note that λ can be considered close to zero since we are concerned by the limit)

$$\frac{1}{\sum_{k=0}^n \lambda^k \rho_k} = \sum_{k=0}^{\infty} \lambda^k \widehat{\rho}_k,$$

that is,

$$\begin{aligned}
1 &= \left(\sum_{k=0}^n \lambda^k \rho_k \right) \left(\sum_{k=0}^{\infty} \lambda^k \widehat{\rho}_k \right) \\
&= \rho_0 \widehat{\rho}_0 + \sum_{k=1}^{\infty} \left(\sum_{j=0}^k \rho_j \widehat{\rho}_{k-j} \right) \lambda^k.
\end{aligned}$$

A recursive formula is then obtained for $\widehat{\rho}_k$

$$\begin{cases} \widehat{\rho}_0 = \frac{-1}{\rho_0} \\ \widehat{\rho}_k = \frac{-1}{\rho_0} \sum_{j=1}^k \rho_j \widehat{\rho}_{k-j}, & \text{for } k = 1, \dots, \infty. \end{cases}$$

Substituted in (17) we get,

$$\begin{aligned}
\left(\frac{1}{\sum_{k=0}^n \lambda^k \rho_k} \right) \partial_x \left(\sum_{k=0}^n \lambda^k p_k \right) &= \left(\sum_{k=0}^{\infty} \lambda^k \widehat{\rho}_k \right) \partial_x \left(\sum_{k=0}^n \lambda^k p_k \right) \\
\left(\frac{1}{\sum_{k=0}^n \lambda^k \rho_k} \right) \partial_y \left(\sum_{k=0}^n \lambda^k p_k \right) &= \left(\sum_{k=0}^{\infty} \lambda^k \widehat{\rho}_k \right) \partial_y \left(\sum_{k=0}^n \lambda^k p_k \right).
\end{aligned}$$

Using the same simplifications as for A_n , we get the following formula for N_n

$$N_n = \begin{cases} A_n = - \sum_{j=0}^n (\partial_x (\rho_{n-j} u_j) + \partial_y (\rho_{n-j} v_j)) \\ B_n = - \sum_{j=0}^n (u_{n-j} \partial_x u_j + v_{n-j} \partial_y u_j + \widehat{\rho}_{n-j} \partial_x p_j) \\ C_n = - \sum_{j=0}^n (u_{n-j} \partial_x v_j + v_{n-j} \partial_y v_j + \widehat{\rho}_{n-j} \partial_y p_j) \\ D_n = - \sum_{j=0}^n (u_{n-j} \partial_x p_j + v_{n-j} \partial_y p_j + \gamma p_j (\partial_x u_{n-j} + \partial_y v_{n-j})). \end{cases} \quad (23)$$

In practice, time integration (18) is, in general, not easy to compute accurately. Indeed, Adomian coefficients N_n are polynomials in time, we need to store all coefficients for an accurate time integration which can be a severe limitation for a large n . The following Theorem remedy this problem, and an exact time integration is obtained by a simple multiplication by time t .

Theorem 1: *The Adomian coefficients N_n can be expressed as*

$$N_n(x, y, t) = t^n \overline{N}_n(x, y), \quad (24)$$

where $\overline{N}_n(x, y)$, depends only on x and y .

Proof: We proceed by induction. The formula is proved for (B_n) and for the other components of N_n the proof can be obtained in a similar way.

Note first that if property (24) is fulfilled by N_n , it is fulfilled by Q_n as well. Indeed

$$Q_{n+1}(x, y, t) = \int_0^t N_n(x, y, s) ds = \frac{t^{n+1}}{(n+1)} \overline{N}_n(x, y) = t^{n+1} \overline{Q}_n(x, y). \quad (25)$$

Note also that the indices of the product terms in $\widehat{\rho}_k$ always sum to k , this implies that $\widehat{\rho}_k$ satisfies the property (24) as long as ρ_k satisfies it, that is

$$\widehat{\rho}_k(x, y, t) = t^k \widehat{\rho}_k(x, y). \quad (26)$$

Now to initialize the induction process, let's verify the property for B_0 and B_1 . From (23) the first Adomian coefficient

$$B_0(x, y, t) = -(u_0 \partial_x u_0 + v_0 \partial_x u_0 + \frac{1}{\rho_0} \partial_x p_0) = t^0 \overline{B}_0(x, y),$$

and then

$$Q_1(x, y, t) = \int_0^t N_0(x, y) ds = t N_0(x, y). \quad (27)$$

The second Adomian coefficient B_1 is given by

$$B_1 = -(u_1 \partial_x u_0 + v_1 \partial_x u_0 + \widehat{\rho}_1 \partial_x p_0 + u_0 \partial_x u_1 + v_0 \partial_x u_1 + \widehat{\rho}_0 \partial_x p_1),$$

and from (26)

$$\widehat{\rho}_1 = t \widehat{\rho}_1(x, y).$$

Substituting $\widehat{\rho}_1$ and Q_1 into B_1 , it clear that $B_1(x, y, t) = t \overline{B}_1(x, y)$.

Now assume property (24) satisfied till index n and let us prove it for $n+1$. Since the relation is valid for index n we have

$$N_n(x, y, t) = t^n \overline{N}_n(x, y)$$

and

$$Q_{n+1}(x, y, t) = \int_0^t N_n(x, y, s) ds = \frac{t^{n+1}}{n+1} \overline{N}_n(x, y) = t^{n+1} \overline{Q}_n(x, y). \quad (28)$$

Substitute the last expression in B_{n+1} formula (23) we obtain

$$\begin{aligned} B_{n+1} &= \sum_{j=0}^n u_{n+1-j} \partial_x u_j + v_{n+1-j} \partial_y u_j + \widehat{\rho}_{n+1-j} \partial_x p_j \\ &= \sum_{j=0}^n [(t^{n+1-j} \overline{u}_{n-j}(x, y)) (\partial_x t^j \overline{u}_{j-1}(x, y)) + (t^{n+1-j} \overline{v}_{n-j}(x, y)) (\partial_y t^j \overline{u}_{j-1}(x, y))] \\ &\quad + (t^{n+1-j} \widehat{\rho}_{n+1-j}) (\partial_x t^j \overline{p}_{j-1}(x, y))] \\ &= \sum_{j=0}^n t^{n+1} [\overline{u}_{n-j}(x, y) \partial_x \overline{u}_{j-1}(x, y) + \overline{v}_{n-j}(x, y) \partial_y \overline{u}_{j-1}(x, y) + \widehat{\rho}_{n+1-j} \partial_x \overline{p}_{j-1}(x, y)] \\ &= t^{n+1} \sum_{j=0}^n [\overline{u}_{n-j}(x, y) \partial_x \overline{u}_{j-1}(x, y) + \overline{v}_{n-j}(x, y) \partial_y \overline{u}_{j-1}(x, y) + \widehat{\rho}_{n+1-j} \partial_x \overline{p}_{j-1}(x, y)]. \end{aligned}$$

This shows that B_{n+1} is a monomial of degree $n+1$ in time with a coefficient depending only on x, y , that is

$$B_{n+1}(x, y, t) = t^{n+1} \overline{B}_n(x, y)$$

which achieves the *proof* of the Theorem. □

III.II. The ABS formula

Using the previous theorem we can derive a formula for Q_{n+1} that doesn't require any time integration, indeed

$$\begin{aligned} Q_{n+1}(x, y, t) &= \int_0^t N_n(x, y, s) ds = \int_0^t t^n \overline{N}_n(x, y) ds \\ &= \frac{t^{n+1}}{n+1} \overline{N}_n(x, y) = \frac{t}{n+1} [t^n \overline{N}_n(x, y)] \\ &= \frac{t}{n+1} N_n(t, x, y), \end{aligned} \quad (29)$$

which leads using (23) to the following recursive formulation for Q_{n+1} that requires no time integration

$$(ABSFormula) \quad Q_{n+1} = \begin{cases} \frac{-t}{n+1} \left[\sum_{j=0}^n (\partial_x(\rho_{n-j}u_j) + \partial_y(\rho_{n-j}v_j)) \right] \\ \frac{-t}{n+1} \left[\sum_{j=0}^n (u_{n-j}\partial_x u_j + v_{n-j}\partial_y u_j + \hat{\rho}_{n-j}\partial_x p_j) \right] \\ \frac{-t}{n+1} \left[\sum_{j=0}^n (u_{n-j}\partial_x v_j + v_{n-j}\partial_y v_j + \hat{\rho}_{n-j}\partial_y p_j) \right] \\ \frac{-t}{n+1} \left[\sum_{j=0}^n (u_{n-j}\partial_x p_j + v_{n-j}\partial_y p_j + \gamma(\partial_x u_{n-j} + \partial_y v_{n-j})p_j) \right]. \end{cases} \quad (30)$$

Note that the formulation 31 provides a fully analytical scheme, depending only on the initial condition and its derivatives of all orders. To calculate analytically the ABS series terms (or Adomian series terms in general), the only way is to express each term Q_n in terms of Q_0 leading to very complicated expressions even for the first few terms of the series. This is the case even for simple problems, as can be verified in [56, 57, 51, 53]. Another handicap, the derivatives are defined in the strong sense, which requires the initial condition to be C^∞ or at least C^K with K being the first truncated term in the Adomian series. Unfortunately, this is not suitable for real-life problems where solutions show in general discontinuities as in the CFD field, the target applications of this paper.

Alternatively, we propose to consider space derivatives in the weak sense and estimate them numerically. Although any numerical method can be used, in this work, the DG method is selected and implemented following the approach proposed by Shu [65]. However, different DG method formulations can be found in the literature, see, for instance, Cockburn [66]. We refer to the obtained numerical scheme by ABS-DG.

Remark

The extension to $3D$ is straightforward since the system of equations is the same with an additional equation for the third momentum component which is similar to other components. Extension to Navier-Stokes equations is straightforward as well, we can easily check the

recursive propriety for viscous terms and get

$$Q_{n+1} = \begin{cases} \frac{-t}{n+1} \left[\sum_{j=0}^n (\partial_x(\rho_{n-j}u_j) + \partial_y(\rho_{n-j}v_j)) \right] \\ \frac{-t}{n+1} \left[\sum_{j=0}^n (u_{n-j}\partial_x u_j + v_{n-j}\partial_y u_j + \hat{\rho}_{n-j}\partial_x p_j) - \mu (\partial_{x^2}u_{k-1} + \partial_{y^2}u_{k-1}) \right] \\ \frac{-t}{n+1} \left[\sum_{j=0}^n (u_{n-j}\partial_x v_j + v_{n-j}\partial_y v_j + \hat{\rho}_{n-j}\partial_y p_j) - \mu (\partial_{x^2}v_{k-1} + \partial_{y^2}v_{k-1}) \right] \\ \frac{-t}{n+1} \left[\sum_{j=0}^n (u_{n-j}\partial_x p_j + v_{n-j}\partial_y p_j + \gamma(\partial_x u_{n-j} + \partial_y v_{n-j})p_j) \right] \end{cases} \quad (31)$$

III.III. Time-adaptive property of the ABS

From eq. (25) we have

$$Q_{n+1}(x, y, t) = t^{n+1}\overline{Q}_n(x, y),$$

and the exact solution is given by the series,

$$Q = \sum_{n=0}^{\infty} Q_n = Q_0 + \sum_{n=1}^{\infty} Q_n = Q_0 + \sum_{n=0}^{\infty} Q_{n+1} = Q_0 + \sum_{n=0}^{\infty} t^{n+1}\overline{Q}_n(x, y).$$

The solution is a power series in time. In practice, the solution is approximated by the first $K + 1$ first terms based on a given tolerance on the truncation error (TE), that is

$$Q(x, y, t) \simeq Q^K(x, y, t) = Q_0(x, y, t) + \sum_{n=0}^{K-1} t^{n+1}\overline{Q}_n(x, y),$$

with TE given by the series residual

$$TE = \sum_{n=K}^{\infty} t^{n+1}\overline{Q}_n(x, y)$$

shows that $K + 1$ is the time-order.

It is clear that once the tolerance fixed, the first neglected term of the series (the order) will not be the same for each position (x, y) and time step t . Consequently, the order is automatically adjusted at each time step and domain position to the needed accuracy.

III.IV. The ABS-DG for LEE

For the LEE case, formula (31) wrote

$$Q_{n+1}(x, y, t) = \frac{-t}{n+1} \left[\mathcal{A}_0(x, y) \frac{\partial}{\partial x} Q_n(x, y, t) + \mathcal{B}_0(x, y) \frac{\partial}{\partial y} Q_n(x, y, t) \right].$$

III.V. Space discretization

Space discretization is achieved by applying the DG method for each term of the ABS series following Shu's approach, see [65] and [67] for details. Blom's extensive work on DG for LEE [64] is a good reference as well.

In the following, zero-order DG case, which corresponds to a finite volume scheme, is however presented, since it will be used subsequently for stability analysis.

Each Q_n term is approximated at the cell center by the average value

$$Q_n(x_i, y_i, t) \simeq \frac{1}{|S_i|} \int_{S_i} Q_n(x, y, t) dS,$$

where S_i is a given cell surface (for a two-dimensional domain). We then get

$$Q_{n+1}(x_i, y_i, t) = \frac{-t}{n+1} \frac{1}{|S_i|} \int_{\partial S_i} \left[\mathcal{A}_0 Q_n(x, y, t) \eta_x + \mathcal{B}_0 Q_n(x, y, t) \eta_y \right] dS$$

$$Q^K = \sum_{n=0}^K Q_n.$$

Q^K is the approximated solution, and K corresponds to the index for which $|Q_K|$ is smaller than a given tolerance.

Approximating fluxes as in the classical finite volume, the ABS-DG zero-order is obtained,

$$(ABS - DG) \begin{cases} Q(x_i, y_i, 0) = Q_0(x_i, y_i) \\ Q_{n+1}(x_i, y_i, t) = \frac{-t}{(n+1)|S_i|} \sum_j F_n^{i,j} \\ Q^K = \sum_{n=0}^K Q_n, \end{cases} \quad (32)$$

where fluxes $F_n^{i,j}$ can be approximated for instance using Lax-Friedrichs formulation

$$F_n^{i,j} = \frac{1}{2} \left(\overline{\mathcal{A}} (Q_n(x_i, y_i, t) + Q_n(x_j, y_j, t)) \eta_x + \overline{\mathcal{B}} (Q_n(x_i, y_i, t) + Q_n(x_j, y_j, t)) \eta_y \right) - \frac{1}{2} \alpha \left((Q_n(x_j, y_j, t) - Q_n(x_i, y_i, t)) \eta_x + (Q_n(x_j, y_j, t) - Q_n(x_i, y_i, t)) \eta_y \right)$$

$$\overline{\mathcal{A}} = \frac{\mathcal{A}_0^i + \mathcal{A}_0^j}{2} \quad \overline{\mathcal{B}} = \frac{\mathcal{B}_0^i + \mathcal{B}_0^j}{2}$$

with indices i, j referring to nodes i and j and $\mathcal{A}_0^i, \mathcal{A}_0^j, \mathcal{B}_0^i, \mathcal{B}_0^j$ to the values of the matrices at the corresponding nodes.

III. VI. Stability Analysis

The stability analysis is performed for the one-dimensional linear wave propagation equation,

$$\frac{\partial u}{\partial t} + a \frac{\partial u}{\partial x} = 0. \quad (33)$$

For such a purpose, a zero-order ABS-DG in space is used. For convenience, the spatial discretization index i is written as a superscript and ABS iteration n as a subscript. This non-standard notation is intended to differentiate ABS iterations from classical finite difference time steps, where n usually refers to the current time level. ABS-DG terms (u_n) using [32](#)

are given by

$$\begin{aligned}
u_0^i &= u(x_i, 0) \\
u_{n+1}^i(t) &= \frac{-t}{n+1} \frac{1}{2h} \left(a(u_n^{i+1} - u_n^{i-1}) - \alpha(u_n^{i+1} - 2u_n^i + u_n^{i-1}) \right) \\
u^K &= \sum_{n=0}^K u_n.
\end{aligned} \tag{34}$$

Round-off errors (ε_n) are also governed by the same equation.

$$\varepsilon_{n+1}^i = \frac{-t}{n+1} \frac{1}{2h} \left(a(\varepsilon_n^{i+1} - \varepsilon_n^{i-1}) - \alpha(\varepsilon_n^{i+1} - 2\varepsilon_n^i + \varepsilon_n^{i-1}) \right). \tag{35}$$

(ε_n) is decomposed into Fourier series and as suggested by *Von Neumann* stability analysis and due to linearity, it is enough to consider each term of the series separately. For simplicity, we keep the same index n and then consider a Fourier series term $\varepsilon_n^i(t) = \beta_n(t)e^{JK_n x_i}$. The solution is then stable if the *Von Neumann* growth rate amplification $G_n = \frac{\varepsilon_{n+1}^i(t)}{\varepsilon_n^i(t)}$ is bounded.

From equation (35) we obtain,

$$\begin{aligned}
G_n &= \frac{-t}{n+1} \frac{1}{2h} \frac{1}{\beta_n e^{JK_n(x_i)}} \left(a \left(\beta_n e^{JK_n(x_i+h)} - \beta_n e^{JK_n(x_i-h)} \right) \right. \\
&\quad \left. - \alpha \left(\beta_n e^{JK_n(x_i+h)} - 2\beta_n e^{JK_n(x_i)} + \beta_n e^{JK_n(x_i-h)} \right) \right) \\
&= \frac{-t}{n+1} \frac{1}{2h} \left(a \left(e^{JK_n(h)} - e^{JK_n(-h)} \right) - \alpha \left(e^{JK_n(h)} + e^{JK_n(-h)} - 2 \right) \right).
\end{aligned} \tag{36}$$

With $\alpha = \frac{1}{2} \frac{h}{t}$,

$$G_n = \frac{-1}{2(n+1)} \left(\frac{t}{h} a \left(e^{JK_n(h)} - e^{JK_n(-h)} \right) - \frac{1}{2} \left(e^{JK_n(h)} + e^{JK_n(-h)} - 2 \right) \right).$$

Note that

$$\begin{aligned}
\left(e^{\frac{JK_n(h)}{2}} - e^{-\frac{JK_n(h)}{2}}\right)^2 &= -4 \sin\left(\frac{JK_n(h)}{2}\right)^2 \\
&= e^{JK_n(h)} + e^{JK_n(-h)} - 2 \\
&= 2j \sin(JK_n(h)) - 2,
\end{aligned}$$

and by substituting into expression (36), and setting $r = \left|\frac{at}{h}\right|$ and $\theta_n = K_n h$, we get

$$\begin{aligned}
G_n &= \frac{-1}{2(n+1)} \left(2rJ \sin(\theta) + 2 \sin\left(\frac{\theta}{2}\right)^2\right) \\
&= \frac{-1}{2(n+1)} \left(4rJ \sin\left(\frac{\theta}{2}\right) \cos\left(\frac{\theta}{2}\right) + 2 \sin\left(\frac{\theta}{2}\right)^2\right) \\
&= \frac{-2 \sin\left(\frac{\theta}{2}\right)}{n+1} \left(rJ \cos\left(\frac{\theta}{2}\right) + 0.5 \sin\left(\frac{\theta}{2}\right)\right),
\end{aligned}$$

and

$$|G_n| = \frac{2 \left|\sin\left(\frac{\theta}{2}\right)\right|}{n+1} \left(\sqrt{r^2 \cos\left(\frac{\theta}{2}\right)^2 + 0.25 \sin\left(\frac{\theta}{2}\right)^2}\right).$$

Now assume that $|r| < \frac{n+1}{\sqrt{2}}$, we have then

$$\begin{aligned}
|G_n| &< 2 \left|\sin\left(\frac{\theta}{2}\right)\right| \sqrt{0.5 \cos\left(\frac{\theta}{2}\right)^2 + \frac{0.25}{(n+1)^2} \sin\left(\frac{\theta}{2}\right)^2} \\
&\leq 2 \left|\sin\left(\frac{\theta}{2}\right)\right| \sqrt{0.5 \cos\left(\frac{\theta}{2}\right)^2 + 0.25 \sin\left(\frac{\theta}{2}\right)^2}.
\end{aligned}$$

In figure 1 the curve of $H(\bar{\theta}) = \left|\sin(\bar{\theta})\right| \left(\sqrt{0.5 \cos(\bar{\theta})^2 + 0.25 \sin(\bar{\theta})^2}\right)$ as a function of

$\bar{\theta} = \frac{\theta}{2}$ is depicted for $0 \leq \bar{\theta} \leq 2\pi$, which shows that

$$r = \left| \frac{at}{h} \right| < \frac{n+1}{\sqrt{2}} \quad \text{implies} \quad |G_n| < 1.$$

We conclude that a classical CFL condition is necessary to stabilize the first ABS term (u_1) of the Adomian decomposition series (16). For the next terms, as n grows, the condition becomes less restrictive. Note that the first term requires a CFL of $1/\sqrt{2}$ instead of the classical $1/2$ for finite volume with Lax-Friedrichs fluxes, which implies a slight improvement of stability.

III.VII. Boundary Conditions

Boundary conditions are imposed on each term of the ABS series. Two relevant boundary conditions for aeroacoustics are considered: non-reflective and slip wall conditions.

Non-reflective boundary condition in LEE is achieved using the characteristics splitting method. An eigenvalue analysis reveals the wave to be removed (negative eigenvalues for reflection), such that by superposition, there are no outgoing waves. This boundary condition is implemented by modifying the local Lax-Friedrichs

$$(\mathcal{A}_0 Q_n \hat{n}_x + \mathcal{B}_0 Q_n \hat{n}_y)^* = \bar{A} \left\{ \left\{ Q_n + \frac{\lambda}{2} [Q_n] \right\} \right\},$$

with $\bar{A} = \{ \{ \mathcal{A}_0 n_x + \mathcal{B}_0 n_y \} \}$ and $[.]$ the jump along the normal \hat{n} ,

to

$$(\mathcal{A}_0 Q_n \hat{n}_x + \mathcal{B}_0 Q_n \hat{n}_y)^* = (\mathcal{A}_0^- n_x + \mathcal{B}_0^- n_y) Q_n^-. \quad (37)$$

Then, we compute eigenvalues and eigenvectors,

$$(\mathcal{A}_0^- n_x + \mathcal{B}_0^- n_y) Q_n^- = R \Lambda R^{-1} \quad \text{with} \quad R = [r1, \dots, r4], \quad (38)$$

and split them into positive and negative contributions,

$$\Lambda = \text{diag}(\lambda_1, \dots, \lambda_4), \quad (39)$$

$$\Lambda = \Lambda^- + \Lambda^+. \quad (40)$$

Finally, the modified background flow is reassembled into the flux by removing negative eigenvalues,

$$(\mathcal{A}_0 Q_n \hat{n}_x + \mathcal{B}_0 Q_n \hat{n}_y)^* = \left(R \Lambda^+ R^{-1} \right) Q_n^-. \quad (41)$$

Slip wall boundary condition is implemented similarly. Each ABS series term is forced to satisfy a standard slip wall boundary condition. The normal to the wall velocity component is set to zero for each stage such that the condition is satisfied for the final solution. Wall cells velocity is modified the standard way by subtracting the normal component,

$$\widehat{u}_n^- = u_n^- - (u_n^- n_x + v_n^- n_y) n_x \quad \widehat{v}_n^- = v_n^- - (u_n^- n_x + v_n^- n_y) n_y. \quad (42)$$

IV. Connection of ABS and RK schemes for the Linear Case

In this section, a connection between the proposed ABS and the Runge-Kutta (RK) schemes is established for the linear case.

Theorem 2: In the linear case the ABS scheme is a time-adaptive Runge-Kutta scheme.

Proof

Consider a first order ODE of the form

$$Y_t = f(t, Y(t)).$$

The general RK approximation of order K to solve numerically such equation is given by

$$Y_{n+1} = Y_n + \Delta t \sum_{i=1}^K c_i k_i$$

where

$$\begin{aligned}
 k_1 &= f(t_n, Y_n) \\
 k_2 &= f(t_n + \alpha_2 \Delta t, Y_n + \Delta t \beta_{21} k_1(t_n, Y_n)) \\
 k_3 &= f(t_n + \alpha_3 \Delta t, Y_n + \Delta t (\beta_{31} k_1(t_n, Y_n) + \beta_{32} k_2(t_n, Y_n))) \\
 &\vdots \\
 k_i &= f(t_n + \alpha_i \Delta t, Y_n + \Delta t (\sum_{j=1}^{i-1} \beta_{ij} k_j)).
 \end{aligned}$$

Now suppose that f is linear and $f(t, Q) = f(Q)$ and $\beta_{kj} = 0$, for $j = 1, k - 2$, β_{kk-1} are not necessary zero. Consequently, the general Runge-Kutta formula wrote

$$Y_{n+1} = Y_n + \Delta t \sum_{i=1}^K c_i k_i \quad (43)$$

with

$$\begin{aligned}
 k_1 &= f(Y_n) \\
 k_2 &= f(Y_n) + \Delta t \beta_{21} f(k_1(Y_n)) \\
 k_3 &= f(Y_n) + \Delta t \beta_{32} f(k_2(Y_n)) \\
 &\vdots \\
 k_i &= f(Y_n) + \Delta t \beta_{ii-1} f(k_{i-1}(Y_n)).
 \end{aligned}$$

Formulate k_i , in terms of $f(Y_n)$

$$\begin{aligned}
k_1 &= f(Y_n) \\
k_2 &= f(Y_n) + \Delta t \beta_{21} f^2(Y_n) \\
k_3 &= f(Y_n) + \Delta t \beta_{32} f^2(Y_n) + (\Delta t)^2 \beta_{32} \beta_{21} f^3(Y_n) \\
&\vdots \\
k_i &= \sum_{k=1}^i [(\Delta t)^{k-1} \Pi_{j=0}^{k-2} \beta_{(i-j)(i-j-1)}] f^k(Y_n)
\end{aligned}$$

with $\Pi_{j=0}^{-1} = 1$, $f^k = \underbrace{f \circ f \circ f \dots \circ f}_{k \text{ times}}$ and $f^1 = f$.

By substituting in eq. (43) we obtain

$$\begin{aligned}
Y_{n+1} &= Y_n + \Delta t \sum_{i=1}^K c_i k_i \\
&= Y_n + \sum_{i=1}^K c_i \sum_{k=1}^i [(\Delta t)^k \Pi_{j=0}^{k-2} \beta_{(i-j)(i-j-1)}] f^k(Y_n).
\end{aligned}$$

Introducing the clipping function

$$E(k, i) = \begin{cases} 1 & \text{if } k \leq i \\ 0 & \text{if not,} \end{cases}$$

RK can be written as

$$Y_{n+1} = Y_n + \sum_{i=1}^K c_i \sum_{k=1}^K E(k, i) [(\Delta t)^k \Pi_{j=0}^{k-2} \beta_{(i-j)(i-j-1)}] f^k(Y_n)$$

such that we can exchange the order of the sums

$$Y_{n+1} = Y_n + \sum_{k=1}^K \sum_{i=1}^K c_i E(k, i) [(\Delta t)^k \Pi_{j=0}^{k-2} \beta_{(i-j)(i-j-1)}] f^k(Y_n)$$

or

$$Y_{n+1} = Y_n + \sum_{k=1}^K (\Delta t)^k \left[\sum_{i=1}^K c_i E(k, i) \left[\prod_{j=0}^{k-2} \beta_{(i-j)(i-j-1)} \right] \right] f^k(Y_n).$$

We can now drop the function E used to permute sums symbols and get

$$Y_{n+1} = Y_n + \sum_{k=1}^K (\Delta t)^k \left[\sum_{i=k}^K c_i \left[\prod_{j=0}^{k-2} \beta_{(i-j)(i-j-1)} \right] \right] f^k(Y_n). \quad (44)$$

Now recall that the LEE equation is given by

$$Q_t = -\mathcal{A}_0(Q) \frac{\partial Q}{\partial x} - \mathcal{B}_0(Q) \frac{\partial Q}{\partial y},$$

therefore

$$f(t, Q) = f(Q) = -\mathcal{A}_0(Q) \frac{\partial Q}{\partial x} - \mathcal{B}_0(Q) \frac{\partial Q}{\partial y}.$$

The ABS for LEE is given by

$$Q_{k+1}(x, y, t) = \frac{-t}{k+1} \left[\mathcal{A}_0(x, y) \frac{\partial}{\partial x} Q_k(x, y, t) + \mathcal{B}_0(x, y) \frac{\partial}{\partial y} Q_k(x, y, t) \right]$$

that can be written as

$$Q_{k+1} = \frac{t}{k+1} f(Q_k),$$

or recursively

$$Q_{k+1} = \frac{t^{k+1}}{(k+1)!} f^{k+1}(Q_0). \quad (45)$$

Now if the ABS series is truncated at term K , using (45) the solution is approximated by

$$Q \simeq Q^K = \sum_{k=0}^K Q_k = Q_0 + \sum_{k=1}^K \frac{t^k}{(k)!} f^k(Q_0).$$

In practice, the ABS is used to estimate Q at $t_n + \Delta t$ given Q at t_n . Then the previous

formula is used by taking $Q_0 = Q(\cdot, t_n)$ then $Q(\cdot, t_{n+1}) = Q^K$ and $t = \Delta t$. We can then write

$$Q(\cdot, t_{n+1}) = Q(\cdot, t_n) + \sum_{k=1}^K \frac{(\Delta t)^k}{(k)!} f^k(Q(\cdot, t_n)). \quad (46)$$

Equation (46) is similar to (44), to make the two expressions identical we need to equate their coefficients, we then obtain the following system

$$\sum_{i=k}^K c_i [\Pi_{j=0}^{k-2} \beta_{(i-j)(i-j-1)}] = \frac{1}{(k)!}, \quad \text{for } k = 1, K.$$

This system has many solutions, and getting one is enough to prove the theorem. To get a solution, coefficients $\beta_{(l)(l-1)}$ can first be set to any values, we obtain then a linear triangular system in c_i that can be solved by back substitution. A typical solution can be $\beta_{(l)(l-1)} = 1$ then we get $c_K = \frac{1}{K!}$, $c_{K-1} = \frac{1}{(K-1)!} - \frac{1}{K!}$, $c_{K-2} = \frac{1}{(K-2)!} - \frac{1}{(K-1)!}$, \dots , $c_{K-i+1} = \frac{1}{(K-i+1)!} - \frac{1}{(K-i+2)!}$ for $i > 1$. The obtained c_i are positive, providing a coherent set of weights for RK method. The order of truncation K will of course vary with time steps and position (x, y) resulting in a time-adaptive RK scheme. This achieves the proof. \square

Note that for the nonlinear case, ABS and RK are different, this can be easily checked for Burgers' equations for instance, by calculating the first ABS terms.

Remark

The ABS for linear case appears to be an efficient and practical way of applying RK thanks to its recursive formulation. Moreover, the order is adaptive, adjusting for each node of the domain and each time step according to the Adomian series remainder. This interesting property guarantees maximum accuracy with optimal cost, as it will be demonstrated further on.

V. Numerical validation and assessment

The proposed ABS-DG scheme is assessed for the linearized (LEE) and nonlinear Euler equations. Results are compared to exact solutions and reference solutions obtained by high-order RK-DG method. Field variables are presented in non-dimensional form, where

reference values are length $L = 1 \text{ m}$, speed of sound $c_0 = 343 \text{ m/s}$ and density $\rho_0 = 1 \text{ kg/m}^3$. Non-dimensional variables are $t^+ = t c_0/L$, $\rho^+ = \rho/\rho_0$, $u^+ = \frac{u}{c_0}$, $v^+ = \frac{v}{c_0}$ and $p^+ = p/(\rho c_0^2)$. [68].

V.I. Linearized Euler Equations (LEE) case

A Gaussian pulse is propagated using linearized Euler equations. A unit amplitude Gaussian pulse is initiated at the center of 10 units wide square, 6000 triangles are used with 0.19 edge length. Time-step size is $dt^+ = 0.1$ ($CFL = 0.5$). ABS series terms are calculated for each cell till the last term value for non-dimensional pressure is smaller than the tolerance value $p_{tol}^+ = \pm 10^{-3}$. Consequently, each cell yield approximation with different time-order (p -adaptivity in time).

This test case is especially interesting for adaptive methods since only one pulse wave needs to be tracked, and then only a small fraction of the cells require high-order approximation leading to a sensitive computational time reduction. Moreover, an analytical solution for a boundless domain is available, allowing an accurate error analysis. The analytical solution for pressure is given by [69]

$$p(x, y, t) = \frac{\varepsilon_1}{2\alpha_1} \int_0^\infty \left[e^{-\xi^2/4\alpha_1} \cos(\xi t) J_0(\xi \eta) \xi \right] d\xi, \quad (47)$$

where $\eta = [(x - Mt)^2 + y^2]^{1/2}$, J_0 is the zero order Bessel function and $\alpha_1 = \ln(2)/b^2 a$, with b known as the half-width of the Gaussian function. We set $\alpha_1 = 1$ ($b = 0.83$) and $\varepsilon_1 = 10^{-5}$ in this simulation.

For the performed tests, the simulation is stopped before the wave reaches the boundary to avoid boundary effects. Grid convergence is then achieved to verify the correct spatial order. In a second test, non-reflecting and wall boundary conditions are imposed as defined in section III.VII

V.I. I. Boundary-Conditions-Free case

The simulation run till $t^+ = 3$, before wave-boundary interaction occurs. Simulations for several spatial interpolation orders –DG3, DG4, and DG5–(DG i referring to the i^{th} order) and several Runge-Kutta orders –RK2, RK4, and RK5– have been carried out. The RK4 scheme is the 3/8-method and RK5 is the Fehlberg method.

As a first comparison Fig.2 depicts pressure distribution of the propagated Gaussian pulse for ABS-DG and RK-DG for orders 0, 1 and 2 in space and RK2. Results are compared to the exact solution. We can see clearly that ABS-DG results fit better the exact solution for order 0 and slightly better for higher order. Recall that the goal of the proposed ABS scheme is to improve the time performance, not accuracy.

For more quantitative assessment, L^2 errors for p^+ relative to exact solution (47) for ABS-DG and RK-DG are reported in table 1. We can see that ABS-DG has an error comparable to the best Runge-Kutta result for all space orders. This demonstrates that ABS-DG successfully achieves higher-order globally in time. Moreover, locally different orders are successfully combined (p -adaptive). Indeed, when $t^+ = 3$, 54 % of the cells require just one ABS iteration; 7 %, two iterations; 36 % three iterations; and 1 % four iterations. The impact of the time adaptivity is clearly shown in table 2 where normalized computation times with respect to RK2-DG3 computational time is reported. We can see that the ABS has almost the same cost as RK2. As a conclusion for this test, ABS is performing as the 5th order Runge-Kutta with a cost of 2nd order Runge-Kutta.

Grid convergence

The grid convergence of ABS-DG is numerically investigated. A wave propagation is simulated for $t^+ = 2$ (0.006 seconds), and compared to analytical solutions. Four different meshes with different sizes are generated. This is done by selecting different edge sizes in SALOME, a tool used for mesh generate in this work [70]. Simulations are stopped at $t^+ = 2$ (0.006 seconds), and the exact (using the exact solution) error is computed. Fig.3 depicts logarithmic curves of error with respect of h size, and for more clarity, curves of different orders are

plotted in separate graphs Fig.4. The dash lines represent the theoretical order, while the solid lines represent the numerical error. The curves show a good agreement, demonstrating the correct order in space for the proposed scheme.

Table 3 shows L^2 errors for a series of ABS-DG simulations and a series of refined edge lengths h . We can see that for orders 3 and 4, superconvergence results are obtained with approximately $P + 2$. For order 5, slightly higher than theoretical convergence is obtained, with superconvergence of order 7 ($P+2$) for the first refinement ($N = 2$). Overall, convergence results match those expected for 2D discontinuous Galerkin [71].

V.I. II. Boundary-Conditions case

The objective of the second part of this test is the validation of the boundary conditions as defined in section III.VII, which consists of imposing BCs for each ABS series term. Since analytical solution (47) is no longer valid for bounded domains, a RK5-DG5 solution is considered as a reference solution computed on a half grid spacing mesh (0.1 length units).

Fig.5 shows ABS-DG3 pressure distribution results compared to the reference solution for wall and non-reflecting BCs at $t^+ = 6$. In table 4 L^2 errors relative to the reference solution for different ABS-DG spatial orders are calculated. Results show a good agreement with the reference solution with an L^2 error of order 10^{-4} for P_5 . This demonstrates the validity of the proposed approach to impose boundary conditions.

V.II. Nonlinear Euler test case

The Mach 3 forward step problem is a well-known benchmark for shock problems. It was introduced half a century ago by Emery [72] to test some discretization schemes and then adopted by many authors to work on shock-capturing schemes. See Woodward and Colella [73] and works cited therein. This test case intends to validate ABS-DG behavior with shocks and rarefaction waves and the p -adaptivity impact.

A wind tunnel with 1 unit height and 3 units length has a 0.2 unit height step located at 0.6 units from the inlet (left side). The tunnel is assumed to be infinitely wide in the direction orthogonal to the computational plane. A fluid with $\gamma = 1.4$, and $p^+ = 1$ is introduced with

velocity $u^+ = 3$ parallel to the wind tunnel. Tunnel walls are implemented as described in section (III.VII). An unstructured mesh consisting of 3704 elements with an average length of 0.04 units is employed.

The unsteady problem for the time range $t^+ = [0, 6]$ is solved. Within this time, it is well known ([72], [73]) that three shock waves and a rarefaction wave are formed. The test case is set up as follows; the unsteady problem is evolved to $t^+ = 4$ time units, so that shock waves are present. Then, a Gaussian mass pulse with a half-width of 0.1 and amplitude of 0.1 is started at $x = 0.3$ and $y = 0.2$, in order to generate a sound mode [74]. Pressure measurements are recorded using two probes located at coordinates $\text{Probe}_1 = \{1, 0.3\}$ and $\text{Probe}_2 = \{2, 0.8\}$ for the time range $t^+ = [4, 6]$

The rarefaction wave is formed in the corner of the step, a singularity point responsible for the creation of an artificial boundary layer may appear if appropriate entropy corrections are not taken [73]. Such an artificial layer can be avoided using a very refined grid as demonstrated by Cockburn and Shu [66] using p^1 and p^2 RK-DG solver. In this work, no such corrections are taken.

The shock waves are caused by the over-expansion of the gas in the step corner. A shock is formed ahead of the step, which evolves to be reflected on the top wall forming an oblique shock, which in turn generates a second oblique shock after reflection on the step. Kelvin-Helmholtz instabilities are not observed in our simulation, due to the mesh resolution, which is three times coarser than the one used in [73]. Finally, the solution slowly evolves until a steady solution is obtained at $t^+ = 12$ [73]. Fig.6 shows the pressure distribution at $t^+ = 4$ for ABS. We can see that shocks are well captured.

p^+ results for RK3-DG3, RK3-DG6, and ABS-DG3 are plotted in Fig.7. The figure shows the pressure at probes 1 and 2 with respect of time. Pure acoustic waves are obtained by subtracting pulse-less simulation from the pulsed one and plotted in Fig.8. We can see that all results are equivalent and agreed, which proves that for the nonlinear case as well ABS is doing as good as high-order RK method in terms of accuracy. In terms of computational time, ABS was twice faster than RK3-DG3. The more significant speed-up was at the initial transition,

where an over-expansion shock wave was initiated on the step. The speed-up falls down after initial shock formation, and of course, ABS is still computationally faster. Fig.9 shows the number of iterations required by ABS at $t^+ = 4$ for a tolerance value $p^+ = \pm 1 \times 10^{-5}$. 16 cells required 3 iterations, 1185 cells two iterations and, finally, 2503 cells required only one iteration. Overall, ABS is 1.7 times faster than RK at $t^+ = 4$.

VI. Conclusions

In this paper, a time-adaptive numerical scheme based on the Adomian decomposition method (ABS) to solve Euler equations is proposed. The objective is to achieve cost-effectiveness by the mean of time adaptivity. The time discretization is obtained using the Adomian decomposition technique, while the discontinuous Galerkin technique is used for space discretization. The derivation of the proposed scheme is described in detail, a recursive formula is proved such that the obtained scheme can be implemented using the existing standard data structures. Many properties are discussed, including stability analysis, connection to Ruge-Kutta method, and boundary conditions. The more important property of the proposed method is its time-adaptive propriety; the order is automatically adjusted at each time step and over the whole space domain reducing the overall processing time, which is the main objective of the paper. This is numerically demonstrated by comparison to the classical RK-DG results.

Acknowledgments

This research is supported by the Basque Government through the BERC 2014-2017 program and by the Spanish Ministry of Economy and Competitiveness MINECO: BCAM Severo Ochoa accreditation SEV-2013-0323. The authors gratefully acknowledge the financial support of Diputación Foral de Bizkaia (DFB) for this research and the whole BCAM-BALTOGAR project on turbomachinery (grant BFA/DFB-6/12/TK/2012/00020). Imanol Garcia de Beristain was funded by the Basque Government Education Department through the Non Doctoral Researcher Formation Program with reference (PRE_2013_1_1216). Lakhdar Remaki was partially funded by the Project of the Spanish Ministry of Economy and Competitiveness with reference MTM2013-40824-P. Alfaisal University grant IRG with reference IRG20411.

References

- [1] Versteeg, H., and Malalasekera, W., 2007. *An Introduction to Computational Fluid Dynamics*, second edition ed. Pearson Education Limited.
- [2] Katate, M., 2013. *I do like CFD, VOL.1, Governing Equations and Exact Solutions*, second edition ed.
- [3] Colonius, T., and Lele, S. K., 2004. “Computational aeroacoustics: progress on nonlinear problems of soundgeneration”. *Progress in Aerospace Sciences*, **40**, pp. 345–416.
- [4] Remaki L., Hassan O., M. K., 2011. “Aerodynamic Computations Using a Finite Volume Method with an HLLC Numerical Flux Function”. *Mathematical Modelling of Natural Phenomena*, **6**(3), 1, pp. 189–212.
- [5] Olander, M., 2011. “CFD simulation of the volvo cars slotted walls wind tunnel”. Master’s thesis, Department of Applied Mechanics, Chalmers University of Technology,.
- [6] Evans, B., Hassan, O., Jones, J., Morgan, K., and Remaki, L., 2011. “Computational fluid dynamics applied to the aerodynamic design of a land-based supersonic vehicle”. *Numerical Methods for Partial Differential Equations*, **27**(1), pp. 141–159.
- [7] Remaki, L., Hassan, O., Evans, B., and Morgam, K., 2014. “Spray drag effect of fluidized sand for a supersonic vehicle”. *Journal of Coupled Systems and Multiscale Dynamics*, **2**(3), October, pp. 169–177.
- [8] Califano, A., and Steen, S., 2009. “Analysis of different propeller ventilation mechanisms by means of rans simulations”. In First International Symposium on Marine Propulsors, Trondheim, Norway,.
- [9] Moshfeghi, M., Song, Y., and Xie, Y., 2012. “Effects of near-wall grid spacing on sst-k-omega model using nrel phase vi horizontal axis wind turbine”. *Journal of Wind Engineering and Industrial Aerodynamics*,, **Volumes 107–108**, August–September, pp. 94–105,.

- [10] Axerio-Cilies, J., and Iaccarino, G., 2012. “An aerodynamic investigation of an isolated rotating formula 1 wheel assembly”. *Journal of Fluids Engineering*, **134**(12).
- [11] Remaki, L., Ramezani, A., Blanco, J. M., and Antolin, J., 2017. “New simplified algorithm for the multiple rotating frame approach in CFD”. *Journal of Fluids Engineering*, **139**(8), pp. 081–104.
- [12] Wang1, B., Okamoto, K., Yamaguchi, K. A., and Teramoto, S., 2014. “Loss mechanisms in shear-force pump with multiple corotating disks”. *Journal of Fluids Engineering*, **136**(8).
- [13] Yelmule, M., and VSJ, E. A., 2013. “CFD predictions of nrel phase vi rotor experiments in nasa/armes wind tunnel”. *International journal of renewable energy research*, **3**(2).
- [14] Singh, K., Mahajan, S., Shenoy, K., Patwardhan, A., and Ghosh, S., 2007. “CFD modeling of pilot-scale pump-mixer: Single-phase head and power characteristics”. *Chemical Engineering Science*, Vol. 22, Issue 5, pp. 1308-1322,.
- [15] Lu X and Xie P and Ingham D and Ma L, 2018. “A porous media model for CFD simulations of gas-liquid two-phase flow in rotating packed beds”. *Chemical Engineering Science*, **189**(2), pp. 123–134.
- [16] Karthikeyan, T., Abdus, S., and Ezhilsabareesh, K., 2016. “Parametric analysis of a tidal current turbine using CFD techniques”. In Renew 2016 2nd International Conference on Renewable Energies Offshore.
- [17] Da-Wen, S., 2019. *Computational Fluid Dynamics in Food Processing*. CRC Press.
- [18] Anandharamakrishnan, C., 2013. *Computational Fluid Dynamics Applications in Food Processing*. SpringerBriefs in Food, Health, and Nutrition.
- [19] Samuelsberg, A., and Hjertager, B. H., 1996. “Computational modeling of gas/particle flow in a riser”. *AIChE Journal*, **42**(6), pp. 1536–1546.

- [20] Lutz, A., 2010. *Numerical Simulations: Examples and Applications in Computational Fluid Dynamics*. InTech.
- [21] Ram, K. R., Yogesh, D., and Jitendra, R., 2018. “A review on applications of computational fluid dynamics”. *International Journal of LNCT*, **2**(6), pp. 2456–9895.
- [22] Evans, B., Jones, J., Morgan, K., Hassan, O., and Remaki, L., 2010. “Computational fluid dynamics applied to the aerodynamic design of a land-bases supersonic vehicle”. *Journal of Partial Differential Equation*, **27**(1), January, pp. 141–159.
- [23] Atmaca, E., Peker, I., and Altin, A., 2005. “Industrial noise and its effects on humans”. *Polish Journal of Environmental Studies*, **14**(6), pp. 721–726.
- [24] Christopher, K. W. T., 1995. “Computational aeroacoustics-issues and methods”. *AIAA journal*, **33**(10), pp. 1788–1796.
- [25] Colonius, T., and Lele, S. K., 2004. “Computational aeroacoustics: Progress on nonlinear problems of sound generation”. *Progress in Aerospace Sciences*, **40**(6), pp. 345–416.
- [26] Lighthill, M. J., 1954. “On sound generated aerodynamically. II. Turbulence as a source of sound”. In *Proceedings of the Royal Society of London A: Mathematical, Physical and Engineering Sciences*, Vol. 222, The Royal Society, pp. 1–32.
- [27] Lighthill, M. J., 1952. “On sound generated aerodynamically. I. General theory”. In *Proceedings of the Royal Society of London A: Mathematical, Physical and Engineering Sciences*, Vol. 211, The Royal Society, pp. 564–587.
- [28] Liever, P. A., West, J. S., and Harris, R. E., 2016. Validation of high-fidelity CFD/CAA framework for launch vehicle acoustic environment simulation against scale model test data. Tech. rep.
- [29] Schulze, M., Hummel, T., Klarmann, N., Berger, F., Schuermans, B., and Sattelmayer, T., 2017. “Linearized euler equations for the prediction of linear high-frequency stability

- in gas turbine combustors”. *Journal of Engineering for Gas Turbines and Power*, **139**(3), pp. 315–325.
- [30] Bissuel, A., Allaire, G., Daumas, L., Barre, S., and Rey, F., 2018. “Linearized Navier–Stokes equations for aeroacoustics using stabilized finite elements: Boundary conditions and industrial application to aft-fan noise propagation”. *Computers & Fluids*, **166**, pp. 32–45.
- [31] Williamschen, M., Gabard, G., and Bériot, H., 2015. “Performance of the DGM for the linearized Euler equations with non-uniform mean-flow”. In 21st AIAA/CEAS Aeroacoustics Conference, p. 3277.
- [32] Xiao-dong, L., Jiang, M., Jun-hui, G., Da-kai, L., Liu, L., and Xiao-yan, L., 2015. “Recent advances of computational aeroacoustics”. *Applied Mathematics and Mechanics*, **36**(1), jan, pp. 131–140.
- [33] Kroll, N., Hirsch, C., Bassi, F., Johnston, C., and Hillewaert, K., 2015. *IDIHOM-Industrialization of High-Order Methods—A Top Down Approach, Notes on Numerical Fluid Mechanics and Multidisciplinary Design.*, Vol. 128. Springer International Publishing Switzerland.
- [34] Brown, J., 2010. “Efficient nonlinear solvers for nodal high-order finite elements in 3D”. *Journal of Scientific Computing*, **45**(1-3), pp. 48–63.
- [35] Huerta, A., Angeloski, A., Roca, X., and Peraire, J., 2013. “Efficiency of high-order elements for continuous and discontinuous Galerkin methods”. *International Journal for numerical methods in Engineering*, **96**(9), pp. 529–560.
- [36] DOLEJsi, V., and FELCMAN, J., 2002. “Anisotropic mesh adaptation for transonic and supersonic flow simulation”. In ALGORITHMY Conference on Scientific Computing, pp. 78–85.

- [37] Peraire, J., Peiró, J., and Morgan, K., 1992. “Adaptive remeshing for three-dimensional compressible flow computations”. *Journal of Computational Physics*, **103**(2), pp. 269 – 285.
- [38] Sørensen, K. A., Hassan, O., Morgan, K., and Weatherill, N. P., 2003. “A multigrid accelerated time-accurate inviscid compressible fluid flow solution algorithm employing mesh movement and local remeshing”. *International Journal for Numerical Methods in Fluids*, **43**(5), pp. 517–536.
- [39] Habashi, W. G., Dompierre, J., Bourgault, Y., Yahia, A. A., Fortin, M., and Vallet, M. G., 2000. “Anisotropic mesh adaptation: Towards user-independent, mesh-independent and solver-independent CFD solutions: Part I: General principles”. *Internat. J. Numer. Methods Fluids*, **32**, pp. 725–744.
- [40] Remaki, L., and Habashi, W., 2006. “3d mesh adaptation on multiple weak discontinuities and boundary layers”. *SIAM J. Sci. Comput.*, **28**(4), Jan., pp. 1379–1397.
- [41] Zander, N., Bog, T., Kollmannsberger, S., Schillinger, D., and Rank, E., 2015. “Multi-level *hp*-adaptivity: high-order mesh adaptivity without the difficulties of constraining hanging nodes”. *Computational Mechanics*, **55**(3), pp. 499–517.
- [42] da Veiga, L. B., Manzini, G., and Mascotto, L., 2018. “A posteriori error estimation and adaptivity in *hp* virtual elements”. *arXiv preprint arXiv:1804.07898*.
- [43] Walter, D. J., and Manera, A., 2016. “Adaptive burnup stepsize selection using control theory for 2D lattice depletion simulations”. *Progress in Nuclear Energy*, **88**, pp. 218–230.
- [44] Völcker, C., Jørgensen, J. B., Thomsen, P. G., and Stenby, E. H., 2010. “Adaptive stepsize control in implicit Runge-Kutta methods for reservoir simulation”. *IFAC Proceedings Volumes*, **43**(5), pp. 523–528.

- [45] Adomian, G., and Rach, R., 1983. “Inversion of nonlinear stochastic operators”. *Journal of Mathematical Analysis and Applications*, **91**(1), pp. 39–46.
- [46] Adomian, G., 1994. “Solving frontier problems of physics: The decomposition method”. *Kluwer Academic Publishers*.
- [47] Cherruault, Y., 1998. *Modèles et méthodes mathématiques pour les sciences du vivant*. Presses Universitaires de France-PUF.
- [48] Ebaida, A., Aljoufia, M. D., and Wazwaz, A. M., 2015. “An advanced study on the solution of nanofluid flow problems via Adomian’s method”. *Applied Mathematics Letters*, **49**, pp. 117–122.
- [49] Duan, J.-S., Rach, R., Baleanu, D., and Wazwaz, A.-M., 2012. “A review of the Adomian decomposition method and its applications to fractional differential equations”. *Communications in Fractional Calculus*, **3**(2), pp. 73–99.
- [50] Wazwaz, A., 2011. *Linear and Nonlinear Integral Equations: Methods and Applications*. Higher Education Press, Beijing.
- [51] Rach, R., Duan, J. S., and Wazwaz, A. M., 2015. “Solving new fourth-order Emden-Fowler type equations by the Adomian decomposition method”. *International Journal of Computational Methods in Engineering Science and Mechanics*.
- [52] Singh, R., and Wazwaz, A., 2015. “An efficient semi-numerical technique for solving nonlinear singular boundary value problems arising in various physical models”. *International J. Of Computer Mathematics*.
- [53] Momani, S., and Odibat, Z., 2006. “Analytical solution of a time-fractional Navier-Stokes equation by Adomian decomposition method”. *Applied Mathematics and Computation*, **177**, pp. 488–494.
- [54] Khan, N., Ara, A., Anwer Ali, S., and Mahmood, A., 2009. “Analytical study of Navier–Stokes equation with fractional orders using He’s homotopy perturbation and variational

- iteration methods”. *International Journal of Nonlinear Sciences and Numerical Simulation*, **10**, 02, pp. 1127–1134.
- [55] Vahidi, A., and Jalalvand, B., 2012. “Improving the accuracy of the adomian decomposition method for solving nonlinear equations”. *Applied Mathematical Sciences*, **6**(10), pp. 487 – 497.
- [56] Gbadamosi, B., Adebimpe, O., Akinola, E. I., and A., O. I., 2012. “Solving Riccati equation using Adomian decomposition method”. *International Journal of Pure and Applied Mathematics*, **78**(3), pp. 409–417.
- [57] Alabdullatif, M., Abdusalam, H. A., and Fahmy, E. S., 2007. “Adomian decomposition method for nonlinear reaction diffusion system of Lotka-Volterra type”. In *International Mathematical Forum*, Vol. 2, pp. 87–96.
- [58] Mohyud-din, S. T., Noor, M. A., and Noor, K. I., 2010. “Variational iteration method for Burgers’ and coupled Burgers’ equations using He’s polynomials”. pp. 263–267.
- [59] Zhu, H., Shu, H., and Ding, M., 2010. “Numerical solutions of two-dimensional Burgers’ equations by discrete Adomian decomposition method”. *Computers & Mathematics with Applications*, **60**(3), pp. 840–848.
- [60] Chen, Y., and An, H. L., 2008. “Numerical solutions of coupled Burgers equations with time- and space-fractional derivatives”. *Applied Mathematics and Computation*, **200**, pp. 87–95.
- [61] Birajdar, G. A., 2014. “Numerical solution of time fractional Navier–Stokes equation by discrete Adomian decomposition method”. *Nonlinear Engineering*, **3**(1), pp. 21–26.
- [62] Rydin, Y., 2016. “Modeling sound propagation from wind turbines using linearized 3d euler equations”. PhD thesis, Uppsala University, Division of Scientific Computing.

- [63] Imanol, G. d. B., 2018. “On adomian based numerical schemes for euler and navier-stokes equations and application to aeroacoustics propagation”. PhD thesis, UPV, University Spain.
- [64] Blom, C. P. A., 2003. “Discontinuous galerkin method on tetrahedral elements for aeroacoustics”. PhD thesis, Ph.D. thesis, University of Twente, Enschede, The Netherlands.
- [65] Shu, C.-W., and Atkins, H. L., 1998. “Quadrature-free implementation of discontinuous Galerkin method for hyperbolic equations”. *AIAA Journal*, **36**(5), May, pp. 775–782.
- [66] Cockburn, B., Karniadakis, G. E., and Shu, C.-W., 1999. “The development of discontinuous Galerkin methods”. *IMA Preprint Series No. 1662*.
- [67] Lummer, M., 2016. “A hybrid 3d discontinuous galerkin code for caa applications”. In 22nd AIAA/CEAS Aeroacoustics Conference, p. 2719.
- [68] Masatsuka, K., 2013. *I do like CFD, VOL.1, Second Edition*. No. v. 1. K. Masatsuka.
- [69] Tam, C., and Webb, J., 1993. “Dispersion-relation-preserving finite difference schemes for computational acoustics”. *Journal of Computational Physics*, **107**(2), p. 262–281.
- [70] Bergeaud, V., and Lefebvre, V., 2010. “Salome. a software integration platform for multi-physics, pre-processing and visualisation”.
- [71] Chalmers, N., 2015. “c”. PhD thesis, University of Waterloo.
- [72] Emery, A. F., 1968. “An evaluation of several differencing methods for inviscid fluid flow problems”. *Journal of Computational Physics*, **2**(3), pp. 306 – 331.
- [73] Woodward, P., and Colella, P., 1984. “The numerical simulation of two-dimensional fluid flow with strong shocks”. *Journal of computational physics*, **54**(1), pp. 115–173.
- [74] Chu, B.-T., and Kovásznyai, L. S. G., 1958. Non-linear interactions in a viscous heat-conducting compressible gas.

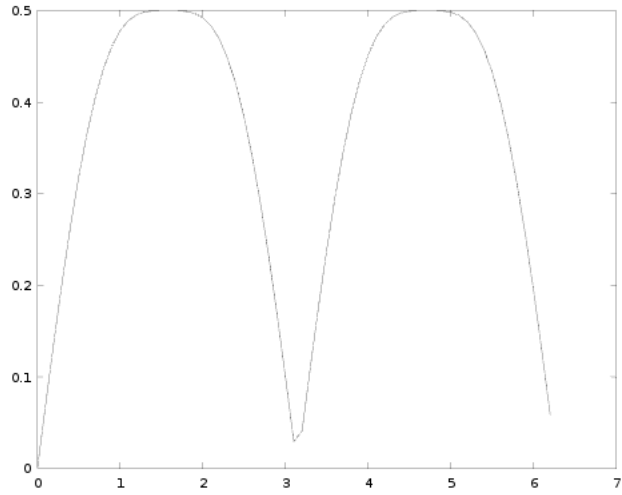
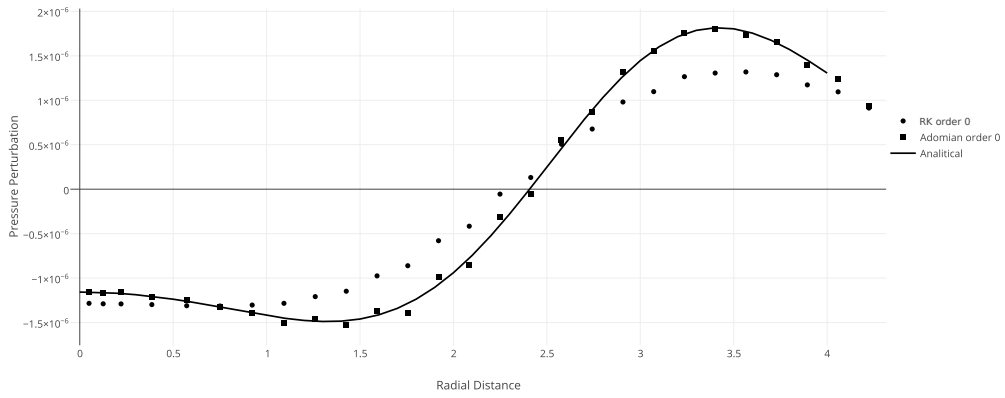
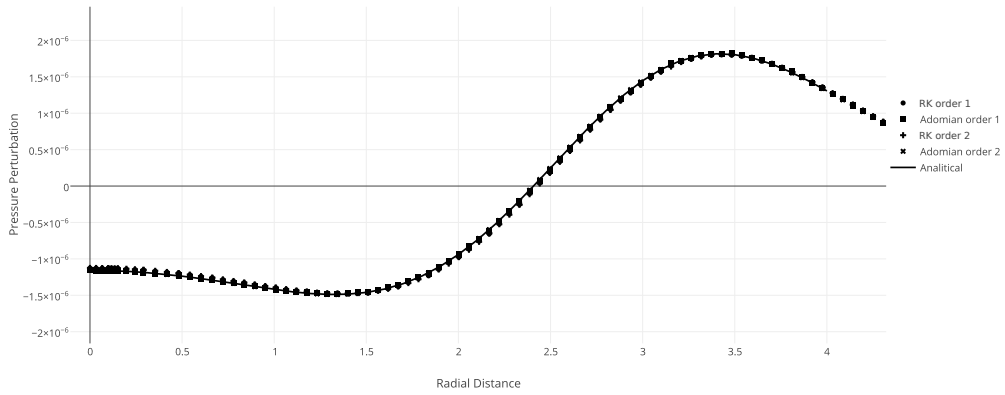


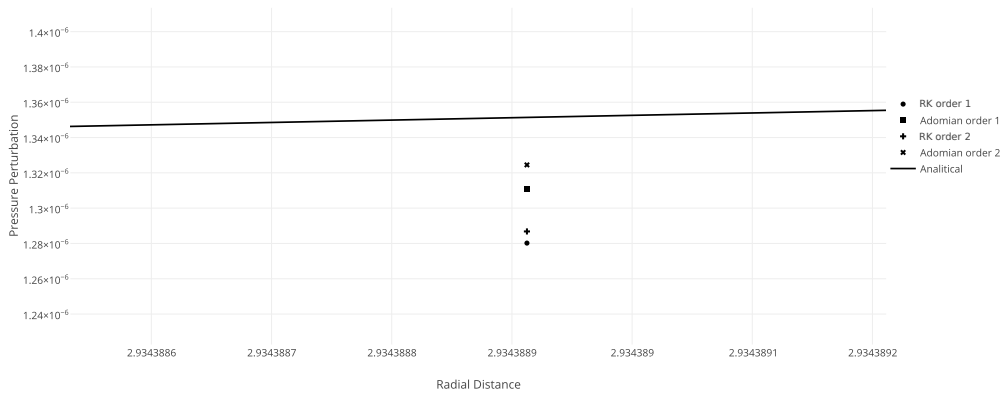
Figure 1: $H(\theta)$ function numerical evaluation



(a) Comparison of the first-order ABS-DG, RK-DG and exact solution



(b) Comparison of the second and third-order ABS-DG and RK-DG results to the exact solution



(c) Zoom on ABS-DG, RK-DG and exact solution

Figure 2: Pressure profiles of ABS-DG, RK-DG and exact solution for different orders

Table 1: ABS and RK $L^2 p^+$ errors for different spatial interpolation order. BC-free case.

Method	P_3	P_4	P_5
RK2	3.45	1.51	0.63
RK4	0.116	2×10^{-3}	1.3×10^{-4}
RK5	0.117	2×10^{-3}	9.5×10^{-5}
ABS	0.122	2×10^{-3}	1.0×10^{-4}

Table 2: Normalized computational time for RK and ABS at different spatial orders

Method	P_3	P_4	P_5
RK2	1.	1.57	2.27
RK4	2.00	3.21	4.68
RK5	3.11	5.00	7.25
ABS	1.1	1.72	2.51

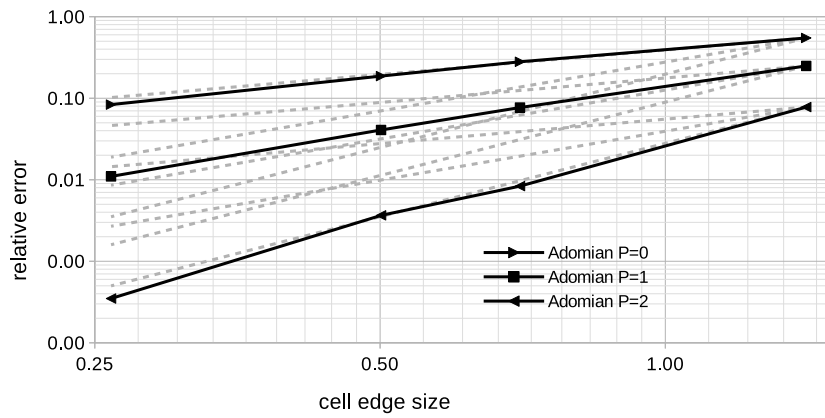
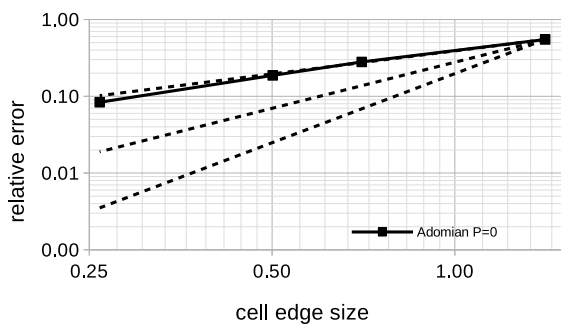
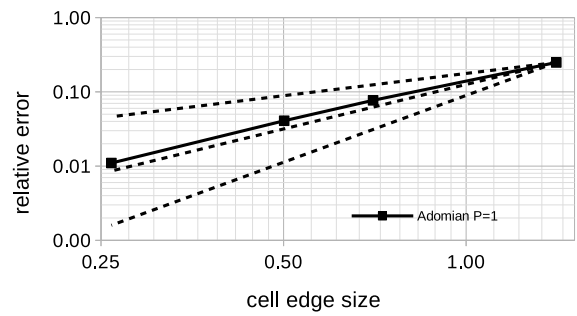


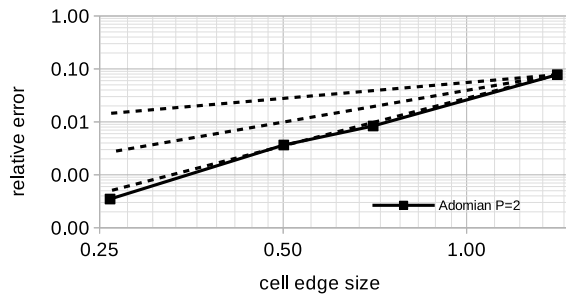
Figure 3: Grid convergence



(a) Grid convergence for order 0



(b) Grid convergence for order 1



(c) Grid convergence for order 2

Figure 4: Grid convergence: Theoretical order curves vs Numerical errors

Table 3: ABS-DG L^2 pressure error [Pa] for different mesh refinements

Order	$N = 1$	$N = 2$	$N = 4$	$N = 8$	conv. order
3	1.794	0.122	1.4×10^{-3}	6.06×10^{-5}	4.93
4	0.545	0.0021	6.0×10^{-5}	2.81×10^{-6}	6.21
5	0.023	0.00017	8.52×10^{-6}	5.19×10^{-7}	5.44

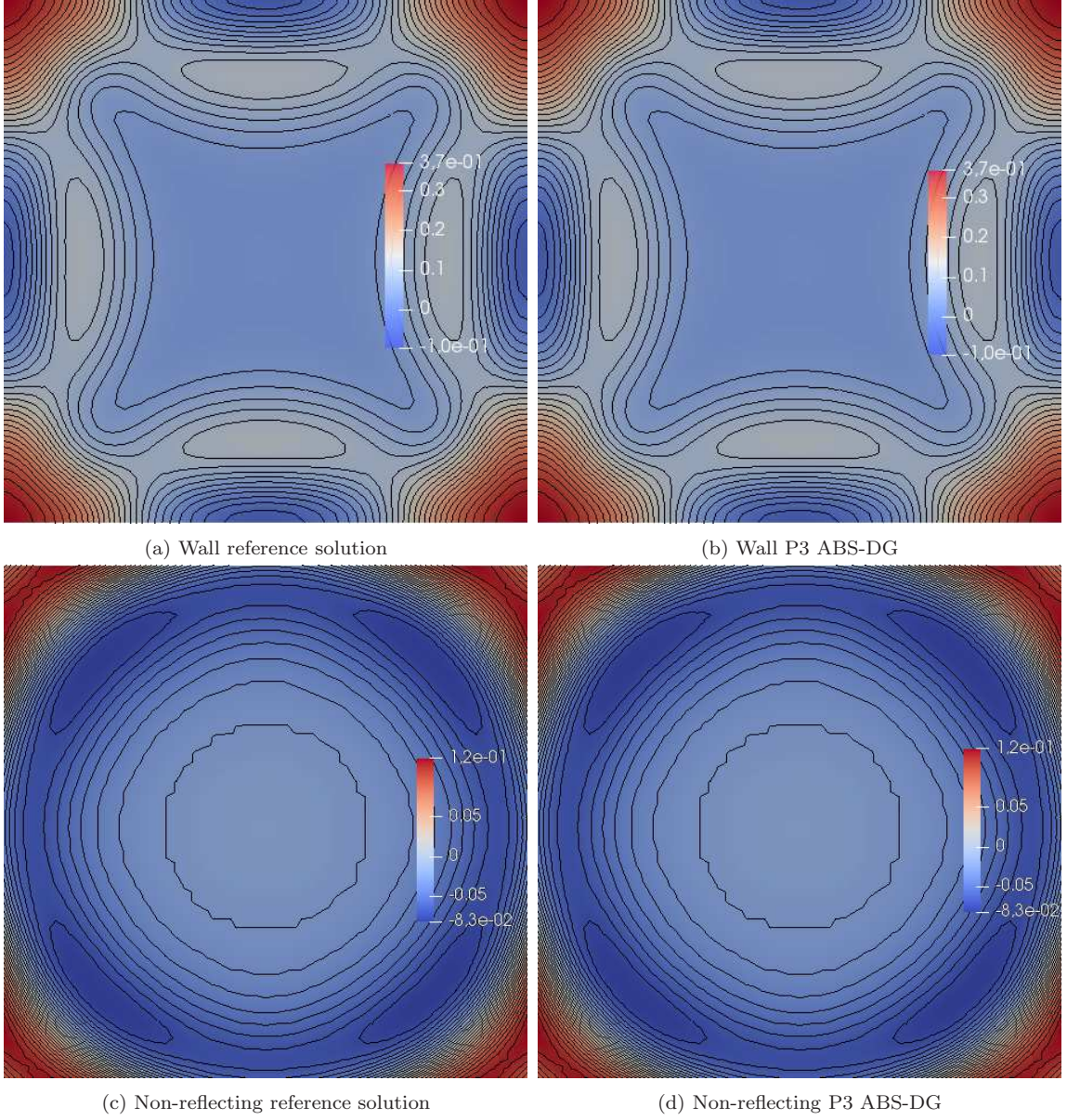


Figure 5: ABS-DG and reference solutions for wall (a and b) and non-reflecting (c and d) boundary conditions at $t^+ = 6$

Table 4: ABS $L^2 p^+$ errors for different spatial interpolation orders. BC case.

BC	P_3	P_4	P_5
non-reflective	1.90	3.2×10^{-3}	1.80×10^{-4}
slip wall	1.96	3.1×10^{-3}	1.82×10^{-4}

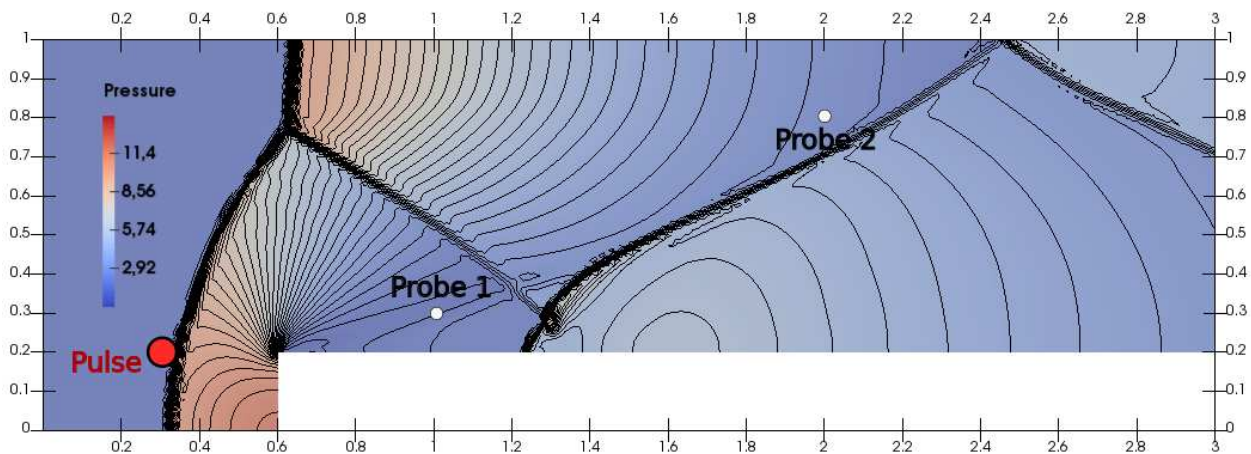


Figure 6: Forward step problem solution at $t^+ = 4$. Contour plots reveal shock waves and a rarefaction wave in the step corner.

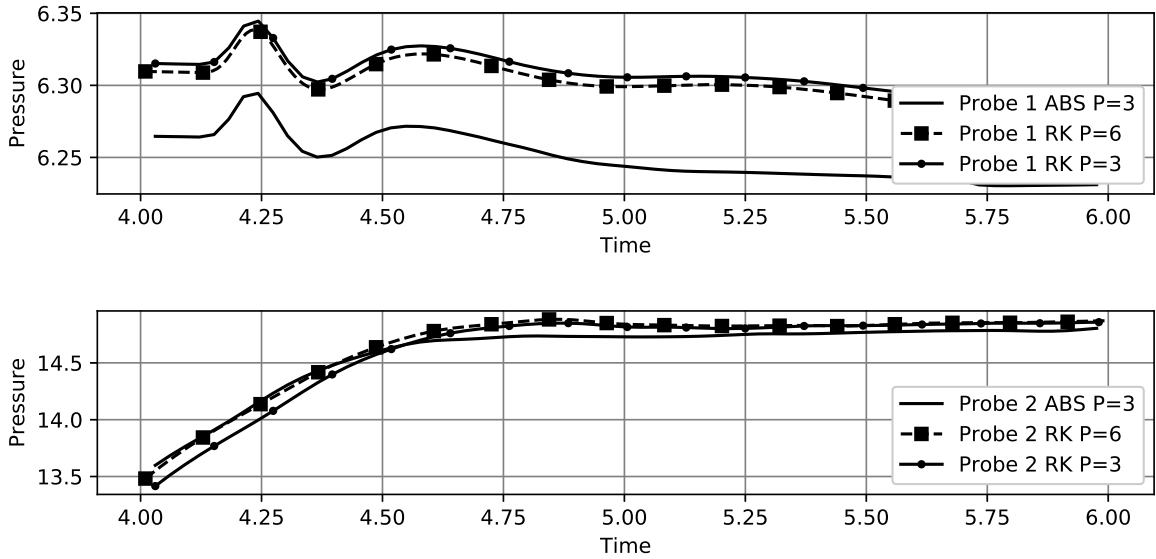


Figure 7: Probe p^+ measurements for RK-DG and ABS-DG.

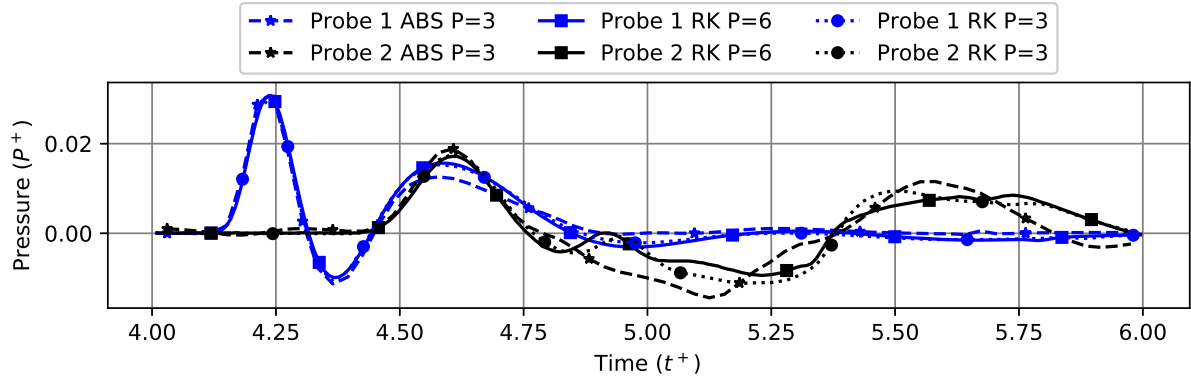


Figure 8: Acoustic mode propagation measured at Probe₁ and Probe₂. Evaluation is done subtracting simulations with initiated Gaussian acoustic pulses at $t^+ = 4$ from pulse-less simulations.

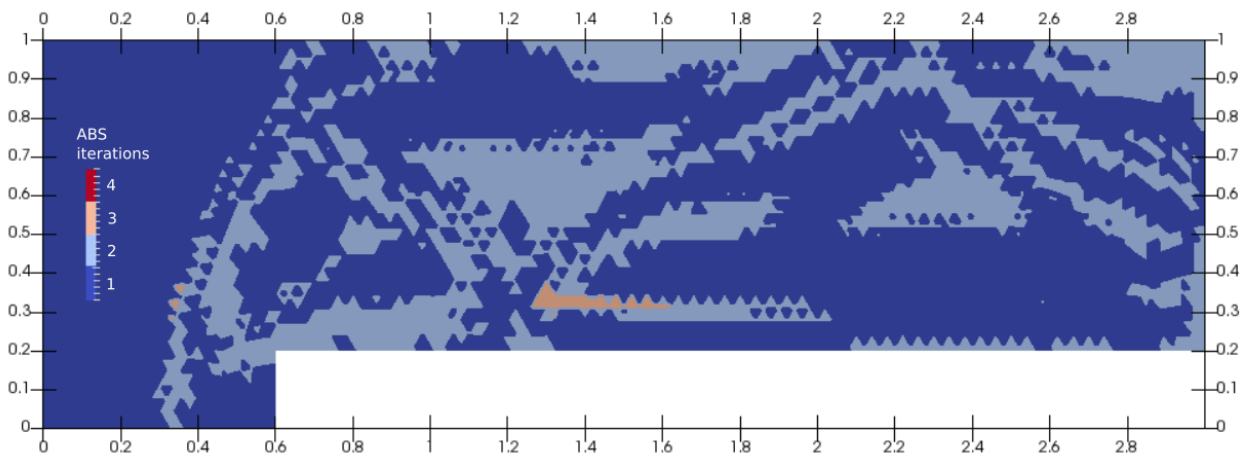


Figure 9: Number of iterations for the forward step problem at $t^+ = 4s$. 2866 cells required 1 iteration, 1357 cells 2 iterations, 75 cells 3 iterations and 0 cells 4 iterations